First-principles investigation of the stability of the oxygen framework of li-rich battery cathodes

First-Principles Investigation of the Stability of the Oxygen Framework of Li-Rich Battery Cathodes

Marnik Bercx, Levi Slap, Bart Partoens and Dirk Lamoen

EMAT & CMT groups, Department of Physics, University of Antwerp, Groenenborgerlaan 171, 2020 Antwerpen, Belgium.

ABSTRACT

Lithium-rich layered oxides such as Li_2MnO_3 have shown great potential as cathodes in Li-ion batteries, mainly because of their large capacities. However, these materials still suffer from structural degradation as the battery is cycled, reducing the average voltage and capacity of the cell. The voltage fade is believed to be related to the migration of transition metals into the lithium layer, linked to the formation of O-O dimers with a short bond length, which in turn is driven by the presence of oxygen holes due to the participation of oxygen in the redox process. We investigate the formation of O-O dimers for partially charged O1-Li_2MnO_3 using a first-principles density functional theory approach by calculating the reaction energy and kinetic barriers for dimer formation. Next, we perform similar calculations for partially charged O1-Li_2IrO_3, a Li-rich material for which the voltage fade was not observed during cycling. When we compare the stability of the oxygen framework, we conclude that the formation of O-O dimers is both thermodynamically and kinetically viable for O1-$Li_{0.5}MnO_3$. For O1-$Li_{0.5}IrO_3$, we observe that the oxygen lattice is much more stable, either returning to its original state when perturbed, or resulting in a structure with an O-O dimer that is much higher in energy. This can be explained by the mixed redox process for Li_2IrO_3, which is also shown from the calculated magnetic moments. The lack of O-O dimer formation in O1-$Li_{0.5}IrO_3$ provides valuable insight as to why Li_2IrO_3 does not demonstrate a voltage fade as the battery is cycled, which can be used to design Li-rich battery cathodes with an improved cycling performance.

INTRODUCTION

Li-ion batteries are currently the primary source of energy storage for many important applications, however many potential gains in energy density can still be made by improving the cathode capacity. Li-rich materials are a promising class of compounds that have demonstrated a high capacity [1]. This increased capacity is believed to be related to the participation of oxygen in the redox processes as the battery is cycled, which has been the topic of extensive investigation. Sathiya *et al.* [2] have discussed the oxidation of oxygen leads to the formation of holes on the oxygen, which are subsequently stabilized by a reorganisation of the oxygen framework, forming a peroxo-like species of oxygen pairs with shortened O-O bonds. This shortened bonding pattern has been subsequently confirmed for Li_2IrO_3 by McCalla *et al.* [3] via a combination of transmission electron microscopy and neutron diffraction. Seo *et al.* [4] have proposed that the formation of

localized holes relies on the presence of labile oxygen states, which are a result of the local oxygen environment.

More recently, several authors have asserted that the presence of unstable holes on the oxygen can also lead to the formation of an oxygen dimer, finding O-O bonds with distances closer to that of molecular oxygen (~1.3-1.5 Å). Such short O-O distances have also been reported recently by Xiang *et al.* [5], who found peaks in their Raman spectra that correspond to similar bond lengths. Both Saubanière *et al.* [6] and Chen and Islam [7] discuss that the dimerization of oxygen can trigger the migration of Mn in fully charged Li_2MnO_3, which is considered to be the mechanism by which the structure transforms into a spinel-type phase. This structural change results in a reduced average voltage, which is detrimental for the energy density of the battery [8]. Moreover, Chen and Islam contend that the O-O dimer is eventually released from the structure as O_2. Such oxygen evolution has been observed for several Li-rich materials [9–11]. Interestingly, McCalla *et al.* found that for Li_2IrO_3, the voltage fade found in Li_2MnO_3 is not observed, and that O_2 release is limited and only occurs at very high states of charge. Understanding why these processes occur for Li_2MnO_3 but not for Li_2IrO_3 can help prevent the degradation of the cathode and open up this class of materials for further development.

So far the study of dimer formation in Li_2MnO_3 has been limited to the O3 stacking and the fully charged structure. However, as Li_2MnO_3 is charged, it is believed to transform into an O1 stacking [12], which changes the possible migration pathways for the transition metal. Such a transformation was also observed for Li_2IrO_3 by McCalla *et al.* In this article we compare the stability of the oxygen framework of Li-rich Li_2MnO_3 and Li_2IrO_3 by calculating the thermodynamic driving force of the dimer formation, as well as the kinetic barrier. The goal is to check if there is a connection between the voltage fade and formation of dimers, induced by the oxidation of oxygen. Instead of investigating the fully charged structures, we apply our methodology to 75% delithiated $Li_{0.5}MnO_3$ and $Li_{0.5}IrO_3$. For the optimal lithium configuration, we find that the oxygen dimer formation is much less likely in Li_2IrO_3, which could explain the lack of voltage fade and oxygen evolution found for this material.

COMPUTATIONAL DETAILS

All calculations are performed in the density functional theory (DFT) framework, as implemented in the Vienna Ab initio Simulation Package (VASP) [13,14]. The projector augmented wave (PAW) method [15] was used to make a distinction between the core and valence electrons, with the standard VASP recommended choice for the number of valence electrons. The wave functions of the valence electrons are expanded in a plane wave basis set, using a high energy cutoff equal to 500 eV, which is advisable for structures containing oxygen. The bulk structures were optimized with the hybrid HSE06 functional [16]. A suitably converged Monkhorst-Pack mesh [17] was chosen for the k-point sampling of the Brillouin zone, with a k-mesh spacing smaller than 0.05 $Å^{-1}$. Geometry optimizations were performed with a Gaussian smearing of 0.05 eV for semiconductor and insulators, and a Methfessel-Paxton [18] smearing of 0.2 eV for metallic structures, followed by a self consistent field calculation using the tetrahedron method [19], for an accurate calculation of the total energies. The convergence criterion on the electronic optimization is set at 10^{-6} eV, and 10^{-3} eV for the geometric optimization. As Ir is known to exhibit a strong spin-orbit interaction, non-collinear calculations including spin-orbit coupling were performed for calculating the magnetic moment and density of states of Li_xIrO_3. The dimer reaction energy and kinetics of both compounds were calculated in a 2x2x2 supercell,

where we switched to the PBE+U functional [20,21] in order to make the dimer screening computationally feasible. A range of choices for the U parameter were tested to closely match the magnetic moments and lattice constants of the HSE06 calculation for the bulk structures, and we settled on 3.9 eV for Mn and 4.0 eV for Ir. Activation energies were calculated using the nudged elastic band (NEB) method [22].

DISCUSSION

In order to compare the structural stability of the oxygen framework for the Li_2MnO_3 and Li_2IrO_3 compounds, we have to calculate the chemical reaction energy for the formation of O-O dimers for both cathode materials in a charged state, i.e. after the removal of a certain concentration of lithium. However, the fully charged structure for Li_2MnO_3 is found to be highly unstable, i.e. lead to the spontaneous formation of several oxygen dimers. Moreover, the cathode is unlikely to ever be fully delithiated in a practical battery. We choose to work with the 75% charged structures, $Li_{0.5}MnO_3$ and $Li_{0.5}IrO_3$, as based on the oxygen evolution we would expect dimerization for this state of charge for Li_2MnO_3 but not Li_2IrO_3. The lithium configuration was found by comparing the energy of all symmetrically non-equivalent configurations in the primitive cell. Similar to previous work [12], we find that for the optimal lithium configuration, the $Li_{0.5}MnO_3$ structure spontaneously shifts from an O3 stacking to the O1 stacking, with the lithium in the 1a Wyckoff sites (Figure 1). A similar transformation is found to occur for $Li_{0.5}IrO_3$, which has been experimentally verified and leveraged in order to study the deformation of the oxygen framework [3]. Note that we refer to oxygen dimers as a local formation of an oxygen pair which are covalently bonded at a distance close to that of the O_2 molecule.

Oxygen oxidation

As the lithium is removed from the cathode, the oxygen of the Li-rich materials is believed to oxidize [23]. To confirm the change in the oxidation state of the atoms, we compare the calculated local magnetic moments of the various elements for both structures in the discharged and 75% charged state in Figure 1 and Table I. We can see that for Li_2MnO_3, the magnetic moment of Mn remains largely the same, whereas the magnetic moment on oxygen increases significantly. For oxygen, the increase in magnetic moment corresponds to an oxidation from its O^{2-} state, as its p-orbitals are no longer fully occupied, leading to an increased local density of unpaired electrons. The results

Table I: Calculated magnetic moments and O-O distances in $Li_2[Mn, Ir]O_3$.

		$Li_2[Mn, Ir]O_3$	$Li_{0.5}[Mn, Ir]O_3$
Mn	$\|\mu\|$(Mn)	2.918 μ_B	2.949 μ_B
	$\|\mu\|$(O)	0.001 μ_B	0.445 μ_B
	d_{short}	2.52 Å	2.31 Å
	d_{long}	2.75 Å	2.61 Å
Ir	$\|\mu\|$(Ir)	0.762 μ_B	1.165 μ_B
	$\|\mu\|$(O)	0.069 μ_B	0.371 μ_B
	d_{short}	2.75 Å	2.51 Å
	d_{long}	2.87 Å	2.74 Å

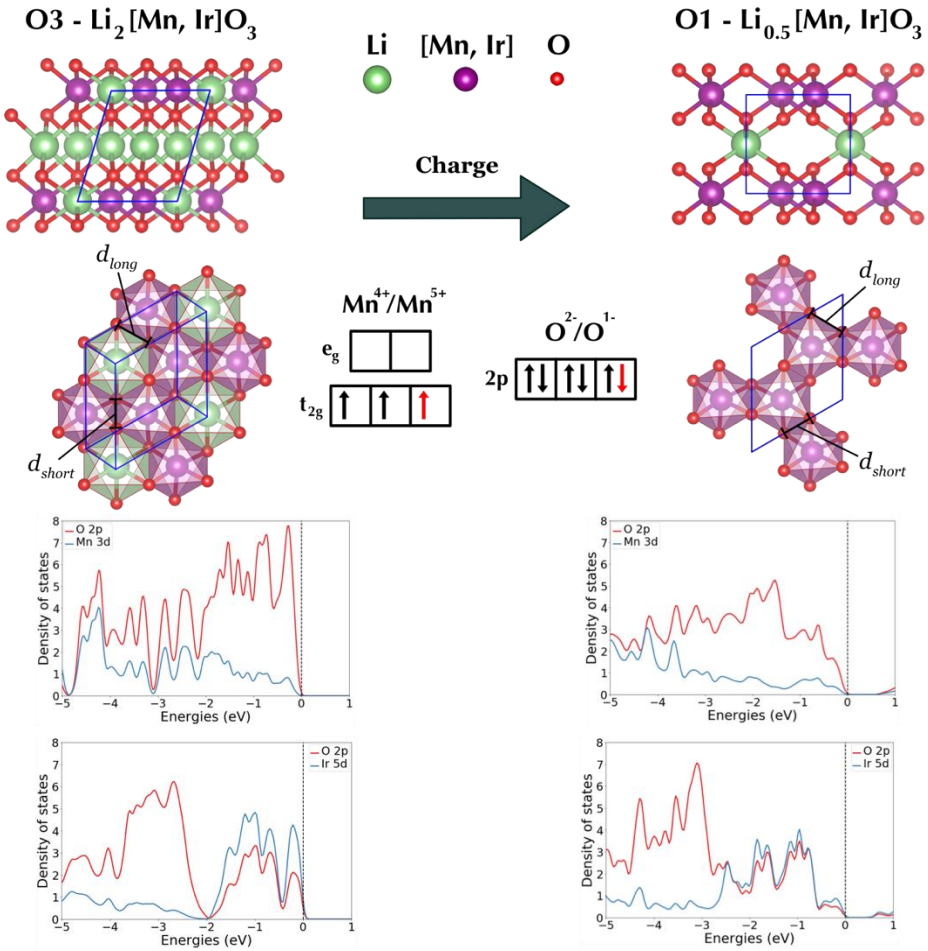

Figure 1: Charging of the $Li_2[Mn, Ir]O_3$ cathode. The unit cell of the HSE06 calculation is drawn in blue. Atomic orbital diagrams are also drawn in order to elucidate the connection between the magnetic moment and the oxidation state for Mn and O. The top figures are the structure shown in the [100] projection, whereas the lower figures represent a single octahedral layer of the layered structure, viewed top down. The projected density of states of the Mn-3d, Ir-5 and O-2p orbitals are also shown for the discharged (left) and charged (right) structure.

for Mn indicate that it does not participate much in the redox processes that occur when the battery is charged. Instead, its magnetic moment remains close to $3\,\mu_B$, which corresponds to the initial oxidation state Mn^{4+} in the discharged cathode structure. For Li_2IrO_3, removing lithium from the discharged structure results in a significant change of the local magnetic moment for both Ir and O, implying a more mixed redox process during the charging of the cathode. This mixed redox for Li_2IrO_3 is in agreement with the XPS results of McCalla *et al.* [3], where they explain that this is in part due to the covalent character of the Ir-O bond. This covalency could also explain why oxygen is oxidized less when charging Li_2IrO_3, as valence electrons are removed from both Ir and O. Mn^{4+} could in principle also be oxidized further, but the Mn^{5+} oxidation state is rare, and generally not octahedrally coordinated [24]. The fact that the change in magnetic moment on O is smaller for Li_2IrO_3 than for Li_2MnO_3 indicates that the mixed redox process in the charging of Li_2IrO_3 results in less oxidation of the oxygen of the structure in the charged state. This is supported by the projected density of states (PDOS), also plotted in Figure 1. For

Li_2MnO_3, the electronic states close to the fermi level correspond largely to the O 2p states. This indicates that as the battery is charged, electrons are removed from oxygen rather than Mn. In contrast, looking at the PDOS for Li_2IrO_3 reveals that the states near the Fermi level are more evenly distributed between O 2p and Ir 5d, which corresponds well to the picture of a more mixed redox activity for this material. When comparing the PDOS of the charged structures with the discharged ones, we note that in both cases the number of O 2p states near the Fermi level has decreased. The different is much more substantial for Li_2MnO_3 versus Li_2IrO_3, once again implying a larger oxidation of oxygen for Li_2MnO_3.

Along with its oxidation, the oxygen framework is distorted as lithium is removed from the structure. In order to quantify this, we determine the distances between the various oxygen pairs, connected in the tetrahedral environment of Mn or Ir. The distances between oxygen pairs which are part of the same oxygen layer change little. However, for the interlayer oxygen pairs, marked in Figure 1, the change in bond length is more pronounced. Moreover, the shorter bonds d_{short}, for an oxygen pair sharing two [Mn, Ir] neighbors, shrink more than the long bonds d_{long}, which share a transition metal and Li or vacancy. This leads to a distortion of the octahedral environment around the transition metals, resulting in short O-O bonds which McCalla *et al.* refer to as dimers. In this work, we will focus our attention on the formation of a peroxo species with a bond length closer to that of the oxygen molecule, as this formation has been derived theoretically for Li_2MnO_3, and believed to be related the migration of Mn and the resulting voltage fade [6].

Dimer analysis

To calculate the chemical reaction energy of the dimer formation, we construct a 2x2x2 supercell of the primitive unit cell, for the O1 stacking of the 75% charged $Li_{0.5}MnO_3$ and $Li_{0.5}IrO_3$ (Figure 2). In order to consistently study the dimer formation, we need to consider all non-equivalent oxygen pairs that have the potential to form a dimer for each material. We use an in-house Python package[1] to find the non-equivalent potential dimers in the structure. This package relies heavily on the pymatgen [25,26] as well as the fireworks [27] packages for the automation of the dimer calculation workflows. In short, all oxygen dimers in the structure are found using a voronoi decomposition to find the neighbors of the various atoms in the unit cell. Once all oxygen dimers have been found, we set up a list for each non-equivalent potential dimer, which contains all the equivalent dimers to this non-equivalent dimer. From each non-equivalent dimer list, we choose one dimer of the unit cell, with the goal of producing a list of inequivalent dimers that is easy to visualize. In the charged O1-$Li_{0.5}MnO_3$ and O1-$Li_{0.5}IrO_3$ structures, we find a total of 6 non-equivalent dimers, shown in Figure 2. For each structure and each potential dimer, we reduce the distance between the oxygen atoms in the dimer pair to 1.4 Å and once again optimize all atomic positions as described in the methods section. To make sure the interaction between the dimers in the periodic boundary conditions approach of VASP is sufficiently small, we have also performed similar calculations in a 3x3x3 supercell, and found the differences between the reaction energies to be smaller than 50 meV for all potential dimers.

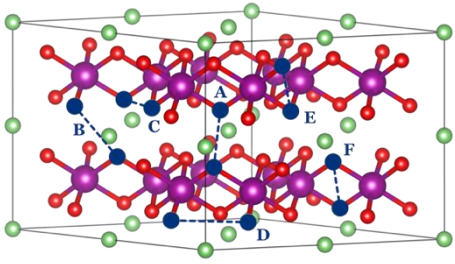

Figure 2: Potential oxygen dimers in O1-$Li_{0.5}$[Mn, Ir]O_3.

[1] Pybat, can be found at https://github.com/mbercx/pybat.

We show the results for the reaction energy and final bond length in Figure 3. Even though all perturbed structures produce a stable oxygen dimer after optimization, only two dimers have a negative reaction energy, which we have labelled as **A** and **E** in Figure 2. One dimer (**C**) results in a geometry similar to the formation of the **E** dimer, with comparable energies. The two dimers that have a reduced energy in the final state are formed by two oxygen atoms from different layers, with dimer **A** being the most energetically favorable by far. We show the final structures both dimers in Figure 3, along with the kinetic barrier, calculated using the NEB method. For the **A** dimer, the kinetic barrier is found to be 214 meV, which is smaller than the typical kinetic barrier for lithium migration in layered structures [28]. This implies that the formation of the **A** dimer is very likely to occur during the charging process. The kinetic barrier for the **E** dimer is significantly higher at 584 meV, but is by no means insurmountable. Hence, we would expect to find both barriers to play a significant role in the structural changes that occur for Li_2MnO_3 as it is cycled.

In stark contrast with the results of O1-$Li_{0.5}MnO_3$, none of the dimer optimizations for O1-$Li_{0.5}IrO_3$ result in a new geometry with a lower energy as the

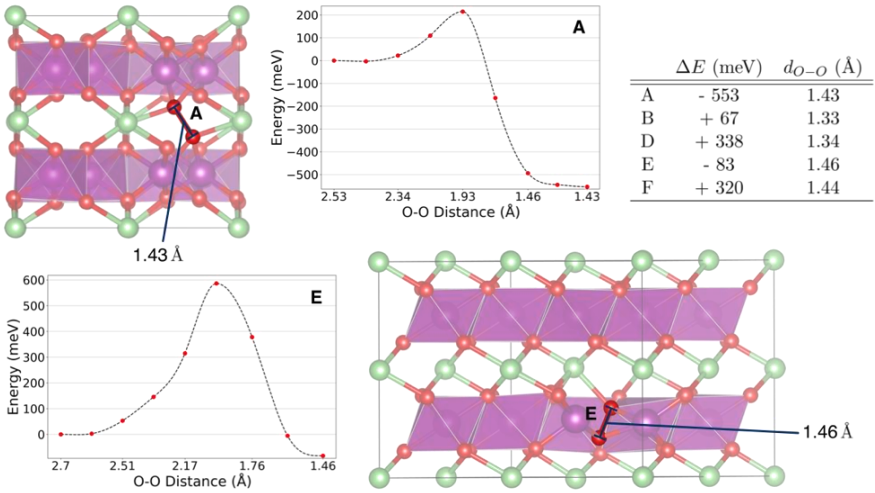

	ΔE (meV)	d_{O-O} (Å)
A	- 553	1.43
B	+ 67	1.33
D	+ 338	1.34
E	- 83	1.46
F	+ 320	1.44

Figure 3: Reaction energies ΔE, final O-O bond length d_{O-O} and kinetic barriers for the dimers in O1-$Li_{0.5}MnO_3$. The final geometry and kinetic barrier is only shown for dimer **A** and **E**, which have a negative reaction energy.

unperturbed structure. In fact, out of all the dimers, all but one return to the original oxygen framework. The only dimer that is stable after optimization has an increased energy of +2.2 eV, and is hence unlikely to be ever formed in practise. In our view, the enhanced stability of the oxygen framework can be in part explained by the reduced participation of oxygen in the redox process as the battery is charged, which is believed to be the primary driver for dimer formation.

CONCLUSION

In this work, we have made a comparison of the stability of the oxygen framework of two layered oxide materials which are being investigated for use as a cathode in Li-ion batteries. Based on a combination of HSE06 and PBE+U calculations, we find that the oxygen lattice is much more stable for Li_2IrO_3 than for Li_2MnO_3, which we believe to be related to the mixed redox activity in Li_2IrO_3. This suggests that introducing transition

metals in the Li-rich structure that allow for higher states of oxidation is a reasonable path for reducing the likelihood of forming O-O dimers, and observing the corresponding structural changes of the cathode that are tied to the detrimental voltage fade and oxygen evolution. Although our results indicate that the formation of oxygen dimers in O1-$Li_{0.5}MnO_3$ is likely to occur, we have yet to study its connection with the migration of Mn into the lithium layer. Other further investigations that could be interesting are the formation of oxygen dimers at the cathode surface, and subsequent evolution of O_2 from the cathode into the electrolyte.

ACKNOWLEDGMENTS

We acknowledge the financial support of FWO-Vlaanderen through project G040116N. The computational resources and services used in this work were provided by the VSC (Flemish Supercomputer Center) and the HPC infrastructure of the University of Antwerp (CalcUA), both funded by the FWO-Vlaanderen and the Flemish Government-department EWI.

References:

[1] Z. Lu, L. Y. Beaulieu, R. A. Donaberger, C. L. Thomas, and J. R. Dahn, J. Electrochem. Soc. **149**, A778 (2002).

[2] M. Sathiya, G. Rousse, K. Ramesha, C. P. Laisa, H. Vezin, M. T. Sougrati, M. L. Doublet, D. Foix, D. Gonbeau, W. Walker, A. S. Prakash, M. Ben Hassine, L. Dupont, and J. M. Tarascon, Nat. Mater. (2013).

[3] E. McCalla, A. M. Abakumov, M. Saubanère, D. Foix, E. J. Berg, G. Rousse, M.-L. Doublet, D. Gonbeau, P. Novák, G. Van Tendeloo, R. Dominko, and J.-M. Tarascon, Science **350**, 1516 (2015).

[4] D. H. Seo, J. Lee, A. Urban, R. Malik, S. Kang, and G. Ceder, Nat. Chem. **8**, 692 (2016).

[5] X. Li, Y. Qiao, S. Guo, Z. Xu, H. Zhu, X. Zhang, Y. Yuan, P. He, M. Ishida, and H. Zhou, Adv. Mater. **30**, (2018).

[6] M. Saubanère, E. McCalla, J. M. Tarascon, and M. L. Doublet, Energy Environ. Sci. (2016).

[7] H. Chen and M. S. Islam, Chem. Mater. (2016).

[8] M. Sathiya, A. M. Abakumov, D. Foix, G. Rousse, K. Ramesha, M. Saubanère, M. L. Doublet, H. Vezin, C. P. Laisa, A. S. Prakash, D. Gonbeau, G. Vantendeloo, and J. M. Tarascon, Nat. Mater. **14**, 230 (2015).

[9] † A. Robert Armstrong, ‡ Michael Holzapfel, ‡ Petr Novák, § Christopher S. Johnson, § Sun-Ho Kang, § and Michael M. Thackeray, and † Peter G. Bruce*, (2006).

[10] E. Castel, E. J. Berg, M. El Kazzi, P. Novák, and C. Villevieille, Chem. Mater. **26**, 5051 (2014).

[11] K. Luo, M. R. Roberts, N. Guerrini, N. Tapia-Ruiz, R. Hao, F. Massel, D. M. Pickup, S. Ramos, Y. S. Liu, J. Guo, A. V. Chadwick, L. C. Duda, and P. G. Bruce, J. Am. Chem. Soc. **138**, 11211 (2016).

[12] Y. Koyama, I. Tanaka, M. Nagao, and R. Kanno, J. Power Sources (2009).

[13] G. Kresse and J. Furthmüller, Phys. Rev. B **54**, 11169 (1996).

[14] G. Kresse and D. Joubert, Phys. Rev. B **59**, 1758 (1999).

[15] P. E. Blöchl, Phys. Rev. B **50**, 17953 (1994).

[16] J. Heyd, G. E. Scuseria, and M. Ernzerhof, J. Chem. Phys. **118**, 8207 (2003).

[17] H. J. Monkhorst and J. D. Pack, Phys. Rev. B **13**, 5188 (1976).

[18] M. Methfessel and A. T. Paxton, Phys. Rev. B **40**, 3616 (1989).
[19] P. E. Blöchl, O. Jepsen, and O. K. Andersen, Phys. Rev. B **49**, 16223 (1994).
[20] J. P. Perdew, K. Burke, and M. Ernzerhof, Phys. Rev. Lett. **77**, 3865 (1996).
[21] S. L. Dudarev, G. A. Botton, S. Y. Savrasov, C. J. Humphreys, and A. P. Sutton, Phys. Rev. B **57**, 1505 (1998).
[22] G. Henkelman and H. Jónsson, J. Chem. Phys. **113**, 9978 (2000).
[23] M. Sathiya, G. Rousse, K. Ramesha, C. P. Laisa, H. Vezin, M. T. Sougrati, M.-L. Doublet, D. Foix, D. Gonbeau, W. Walker, A. S. Prakash, M. Ben Hassine, L. Dupont, and J.-M. Tarascon, Nat. Mater. **12**, 827 (2013).
[24] J. A. Saint, M. M. Doeff, and J. Reed, J. Power Sources **172**, 189 (2007).
[25] S. P. Ong, W. D. Richards, A. Jain, G. Hautier, M. Kocher, S. Cholia, D. Gunter, V. L. Chevrier, K. A. Persson, and G. Ceder, Comput. Mater. Sci. **68**, 314 (2013).
[26] A. Jain, G. Hautier, C. J. Moore, P. Ong, C. C. Fischer, T. Mueller, K. A. Persson, and G. Ceder, Comput. Mater. Sci. **50**, 2295 (2011).
[27] A. Jain, S. P. Ong, W. Chen, B. Medasani, X. Qu, M. Kocher, M. Brafman, G. Petretto, G.-M. Rignanese, G. Hautier, D. Gunter, and K. A. Persson, Concurr. Comput. Pract. Exp. **27**, 5037 (2015).
[28] A. Van Der Ven, J. Bhattacharya, and A. A. Belak, Acc. Chem. Res. (2013).